# Machine learning enabled information fusion of heterogeneous sensing for infrastructure monitoring

## Final Report
## July 2025

**Principal Investigator:** Jiong Tang

Department of Mechanical Engineering
University of Connecticut

**Author:** Jiong Tang, Ting Wang, Yang Zhang, Qianyu Zhou

**Sponsored By**
Transportation Infrastructure Durability Center
List other Sponsors if applicable (i.e. MaineDOT)


**A report from**
University of Connecticut
Department of Mechanical Engineering
191 Auditorium Road
Storrs, CT 06269
Phone: (860) 486 5911
Website: https://dscl.uconn.edu

## About the Transportation Infrastructure Durability Center

The Transportation Infrastructure Durability Center (TIDC) is the 2018 US DOT Region 1 (New England) University Transportation Center (UTC) located at the University of Maine Advanced Structures and Composites Center. TIDC's research focuses on efforts to improve the durability and extend the life of transportation infrastructure in New England and beyond through an integrated collaboration of universities, state DOTs, and industry. The TIDC is comprised of six New England universities, the University of Maine (lead), the University of Connecticut, the University of Massachusetts Lowell, the University of Rhode Island, the University of Vermont, and Western New England University.

## U.S. Department of Transportation (US DOT) Disclaimer



## Acknowledgements

Funding for this research is provided by the Transportation Infrastructure Durability Center at the University of Maine under grant 69A3551847101 from the U.S. Department of Transportation's University Transportation Centers Program. [Include any acknowledgements for other contributors (i.e. your university or contributing DOTs/industry partners) here.]

## Technical Report Documentation Page

| | | |
|---|---|---|
| **1. Report No.** | **2. Government Accession No.** | **3. Recipient Catalog No.** |
| **4 Title and Subtitle**<br>Machine learning enabled information fusion of heterogeneous sensing for infrastructure | | **5 Report Date**<br>**6 Performing Organization Code** |
| **7. Author(s)**<br>Jiong Tang https://orcid.org/0000-0002-6825-9049<br>Yang Zhang, Ting Wang, and Qianyu Zhou | | **8 Performing Organization Report No.** |
| **9 Performing Organization Name and Address**<br>University of Connecticut, Storrs, CT 06269 | | **10 Work Unit No. (TRAIS)**<br>**11 Contract or Grant No.** |
| **12 Sponsoring Agency Name and Address** | | **13 Type of Report and Period Covered**<br>**14 Sponsoring Agency Code** |

**15 Supplementary Notes**

16 **Abstract** In this research, we develop a framework for machine learning enabled information fusion for infrastructure health monitoring. Traditionally, off-the-shelf sensors such as accelerometers and strain gages have been used to collect real-time measurements of structural responses to facilitate health monitoring. While certain levels of successes have been achieved, they also exhibit limitations such as relatively low detection sensitivity to incipient damage and especially limited detection range and coverage. In this project, we 1) establish a benchmark testbed that incorporates various sensors to assess different sensing mechanisms; 2) develop a machine learning based approach that can leverage sensing information and extrapolate to full-field measurement; and 3) investigate scalability strategies that can result in actual implementation of the new framework. Potential applications are large-scale infrastructure such as bridges.

**17 Key Words** Structural damage identification, sensor, inverse analysis, sensor network optimization, full-field measurement, machine learning.

**18 Distribution Statement**
No restrictions. This document is available to the public through

| | | | |
|---|---|---|---|
| **19 Security Classification (of this report)**<br>Unclassified | **20 Security Classification (of this page)**<br>Unclassified | **21 No. of pages**<br>26 | **22 Price** |

Form DOT F 1700.7 (8-72)

# Contents

**List of Figures** ..... 4
**List of Tables** ..... 4
**List of Key Terms** ..... 5
**Abstract** ..... 5
**Chapter 1: Introduction and Background** ..... 6
**1.1 Project Motivation** ..... 6
**1.2 Research, Objectives, and Tasks** ..... 6
**1.3 Report Overview** ..... 7
**Chapter 2: Methodology** ..... 8
**2.1 Materials** ..... 8
**2.2 Test Setup & Process** ..... 8
**Chapter 3: Results and Discussion** ..... 10
**3.1 Full-field reconstruction overview** ..... 10
**3.2 Full-field reconstruction case demonstration** ..... 14
**3.3 Application to Structural Damage Detection** ..... 20
**Chapter 4: Education Impact and Knowledge Dissemination** ..... 23
**Chapter 5: Conclusions and Recommendations** ..... 24
**References** ..... 25

## List of Figures

Figure 1.Experimental setup. ..... 8
Figure 2.Excitation and measurement data flow..... 9
Figure 3.Flowchart of full-filed structural response reconstruction using limited data..... 12
Figure 4.(a) Initialized dictionary and (b) learned dictionary for burst chirp excitation. ..... 15
Figure 5. Multiple optimal solutions for limited sensor layout. ..... 15
Figure 6. Average similarity comparison between different solutions ..... 17
Figure 7. Vibration comparison with ground truth. Blue solid line is ground truth, and orange dash line is reconstruction. The subplots, arranged from the upper left to the bottom right, correspond to measurement locations 1 through 16. ..... 17
Figure 8. Schematic diagram for reconstructions under varying loadings. ..... 18
Figure 9. Response comparisons and error analysis for case of burst to sine. Reconstructed response comparisons using Solution 4 with 6 sensors. ..... 19
Figure 10. (a) Initial dictionary and (b) learned dictionary for sine excitation..... 19
Figure 11. Response comparisons and error analysis for case of sine to burst. Reconstructed response comparisons using Solution 6 with 8 sensors. ..... 20
Figure 12. Schematic illustration of simulation modeling. ..... 21
Figure 13. Damage localization indicators using partial and fully reconstructed responses. ..... 21

## List of Tables

Table 1.Local search heuristics. ..... 13
Table 2. Sensor placement combinations from optimization and perturbations for Case I. ..... 16
Table 3. Performance comparisons on Case I data. ..... 18

## List of Key Terms

*Structural damage identification, sensor, inverse analysis, sensor network optimization, full-field measurement, machine learning.*

## Abstract

*In this research, we develop a framework for machine learning enabled information fusion for infrastructure health monitoring. Traditionally, off-the-shelf sensors such as accelerometers and strain gages have been used to collect real-time measurements of structural responses to facilitate health monitoring. While certain level of successes have been achieved, they also exhibit limitations such as relatively low detection sensitivity to incipient damage and especially limited detection range and coverage. In this project, we 1) establish a benchmark testbed that incorporates various sensors to assess different sensing mechanisms; 2) develop a machine learning based approach that can leverage sensing information and extrapolate to full-field measurement; and 3) investigate scalability strategies that can result in actual implementation of the new framework. Potential applications are large-scale infrastructure such as bridges.*

# Chapter 1: Introduction and Background

## 1.1 Project Motivation

While various sensors and sensing technologies have been developed in recent years to facilitate the structural health monitoring (SHM) of infrastructure, the actual implementation of these new technologies has been limited. Major technical barriers exist. Traditionally, off-the-shelf sensors such as accelerometers and strain gages are employed. Coupled with statistical analysis or model-based dynamic analysis, the changes of local strain or global vibration properties such as natural frequencies, mode shapes, mode shape curvatures, can be used to infer damage occurrence. These approaches however generally suffer from low detection sensitivity. The strain gages would have to be very closed to damage site to detect damage occurrence. The damage would need to be quite severe to induce significant changes to dynamic properties. To tackle such challenges, in recent years a number of new sensing mechanisms have been suggested, including piezoelectric transducers as well as magneto-mechanical transducers for wave propagation and impedance based fault detection. Nevertheless, such high detection sensitivity comes with a price. That is, small variations in the infrastructure under normalcy condition may be diagnosed as fault condition, leading to frequent false alarms. To overcome these technical barriers, we propose to conduct information fusion of sensors and to leverage machine learning to acquire full-field measurement information based on a small number of point sensors.

## 1.2 Research, Objectives, and Tasks

The overarching goal of this research is to synthesize a new framework of infrastructure monitoring that can concurrently take in sensing signals from both traditional sensors and new sensing techniques, process the information through machine learning that integrate together deep learning and underlying physics, and produce highly accurate and robust full field measurement results to facilitate fault detection. These represent paradigm-shifting advancements with respect to the current practice: 1) heterogeneous sensing allows the possibility of taking advantage of the merits of various sensors and avoiding their drawbacks; 2) as more information is processed, the result will be naturally more accurate and robust; 3) the inference of full-field measurement results will significantly enhance the fault detection sensitivity and robustness, and 3) with the machine learning approach, there will be no need to develop complex finite element model of the structure to be inspected, and empirical knowledge can be incorporated into decision making through the adoption of a composite convolutional network architecture to be formulated in this research. As physics knowledge can be injected into the decision making through the new deep learning approach proposed, the methodology can potentially be scalable to large infrastructure with many sensor types and units.

To accomplish these objectives, research activities along two thrust areas are executed, a) testbed setup and data acquisition, b) analysis and machine learning synthesis. Four tasks are conducted:

Task 1: Testbed setup
Task 2: Data acquisition and initial analysis of the testbed
Task 3: Full-field measurement inference
Task 4: Fault detection decision making

## 1.3 Report Overview

In the subsequent chapters, we present the research methodology and results obtained throughout this research.

Chapter 2 outlines the materials involved in this research. The testbed design and analyses are based upon benchmark frame structure experimental investigation. Full field measurement inference is conducted based on the testbed structure.

Chapter 3 presents in detail the research tasks as well as the key data/results. The full field measurement expansion methodology is outlined, followed by damage detection illustrations.

Chapter 4 summarizes the workforce training aspect of the project as well as knowledge dissemination.

Chapter 5 provides the overall conclusion as well as recommendation for future work

# Chapter 2: Methodology

## 2.1 Materials

In terms of physical materials, this project involves a three-story frame structure used as benchmark testbed, a modal shop shaker (K2110E), and a scanning laser Doppler vibrometer (Polytec 500).

In terms of reporting materials, in this final report we provide details of

a) Testbed design details;
b) Modal testing and full-field measurement results;
c) Re-construction of full-field measurement based on point sensing information; and
d) structural damage detection examination cases.

## 2.2 Test Setup & Process

A number of testings are conducted throughout this project. Figure 1 shows testbed setup. Figure 2 details the excitation and measurement data flow.

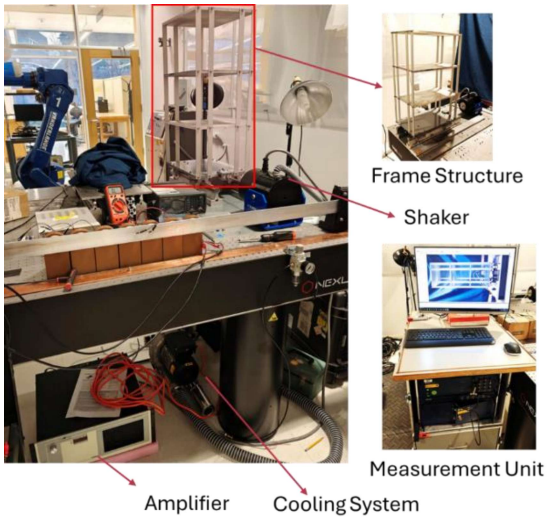


Figure 1.Experimental setup.

The experimental setup comprises two main components: a building structure equipped with 16 accelerometers and excited by a shaker system and a scanning vibrometer capable of dense measurement for validating the full-field reconstruction. Given the use of a 2D laser vibrometer and the symmetry of the frame structure, measurements are conducted on one side of the frame, as indicated in Figure 2. This setup allows us to characterize the full vibrational responses of the structure using 16 sensors. The objective is to estimate the full responses of the frame structure from limited sensor data. In other words, we aim to answer the question: Can a small number of sensors be used to reconstruct the full vibrational responses? The proposed approach follows two main steps: collecting dense measurements from all 16 nodes as prior knowledge (training dataset) and reconstructing the responses under different loading conditions using limited sensor data. It is worth noting that determining the optimal number and placement of sensors is a multi-objective optimization problem, as formulated in the previous section. The adapted optimizer for binary optimization is utilized to solve the problem.

The Polytec 500 vibrometer functions as both a signal generator and a data acquisition system. Different excitation signals are applied via the shaker amplifier (Modal Shop 2050E09-FS), as demonstrated in the next subsection. The shaker (Modal Shop K2110E) is attached to a steel table with a stinger, inducing motion in a single direction, as shown in Figure 5. The frame structure is mounted on the steel shake table, enabling back-and-forth vibrations along one direction when excited. The laser vibrometer captures these vibrations by measuring points marked in Figure 5. The training dataset comprises acceleration responses from 16 nodes, with each time series containing 800 data points.

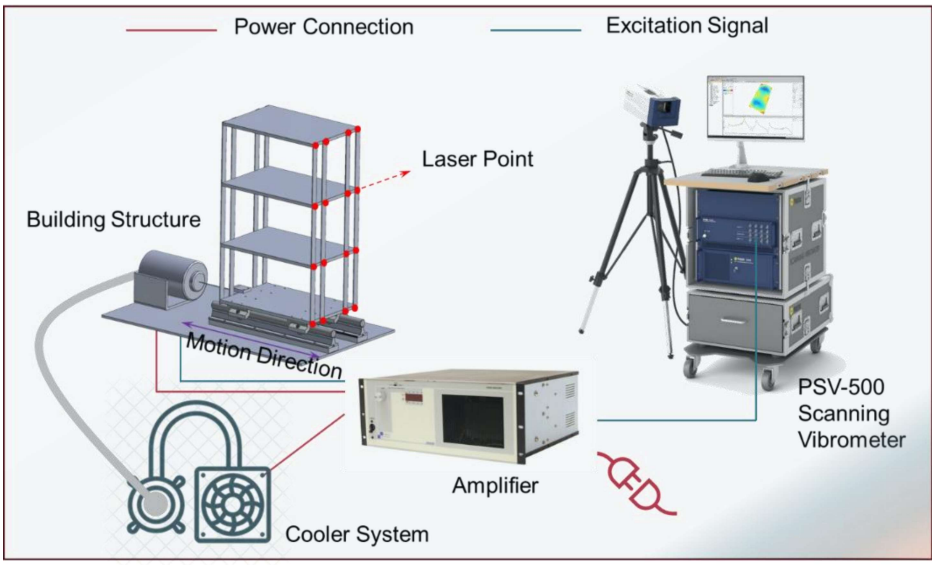


Figure 2.Excitation and measurement data flow

The details of the analyses and testings are reported in Chapter 3.

# Chapter 3: Results and Discussion

## 3.1 Full-field reconstruction overview

The dependence of limited sensor selection can affect the influence the reconstruction performance. Moreover, selecting a few measurement points from all possible points in the full field constitutes a sparse, combinatorial optimization problem. Therefore, this research explores whether this process can be delegated to an optimization algorithm, allowing the algorithm to determine the optimal data volume while maintaining high reconstruction accuracy. Additionally, the process of transitioning from sparse measurements to full-field reconstruction is an underdetermined problem, indicating that multiple solutions are feasible. To fit this nature, this section converts the reconstruction process into a binary multi-objective optimization problem. Subsequently, the sparsity aware MOPSO algorithm enhanced by reinforcement learning is adapted to solve the binary setting.

### 3.1.1 Methodology outline

In data analysis, an effective representation should emphasize the underlying content of signals while reducing redundancy. Sparse representation has emerged as a widely recognized approach, where a signal is reconstructed using only a few dominant components selected from a larger dictionary. A signal $\mathbf{y} \in \mathbb{R}^m$ can often be represented in a sparse manner using a combination of elements from a predefined dictionary. Mathematically, this can be expressed as:

$$\mathbf{y} = \mathbf{D}\mathbf{x} = \sum_{j=1}^{n} x_j \mathbf{d}_j = \sum_{j \in S} x_j \mathbf{d}_j \tag{1}$$

where $\mathbf{D} \in \mathbb{R}^{m \times n}$ is the orthonormal basis matrix or dictionary, and $\mathbf{d}_j$ is the $j$th column of $\mathbf{D}$. $S$ is the total columns of $\mathbf{D}$ (i.e., the number of atoms). In general, the basis matrix is overcomplete. i.e., $m < n$. In Equation (1), most of the coefficients of $x_j$ are zero, hence $\mathbf{x} \in \mathbb{R}^n$ is a sparse vector. The basis matrix $\mathbf{D}$ is chosen in such a way that the signal has a sparse representation in that domain. Most periodic signals or images have a sparse representation in Fourier or wavelet domain. If there is no information available about the signals, then the basis matrices can be obtained via training signals using dictionary learning (Rubinstein et al, 2008; Jana, et al, 2023; Mousavi et al, 2023).

The objective of this study is to find out $\mathbf{y} \in \mathbb{R}^m$ using compressive sensing, which is effectively applied to various applications (Ao et al, 2023; Wei et al, 2023; Yuan et al, 2024), by using limited measurement $\mathbf{z} \in \mathbb{R}^p$. Here, $p << m$. Any measured vector $\mathbf{z}$ is a simple linear projection of the main signal $\mathbf{y}$ and can be found out as

$$\mathbf{z} = \boldsymbol{\theta}\mathbf{y} = \boldsymbol{\theta}\mathbf{D}\hat{\mathbf{x}} = \boldsymbol{\varphi}\hat{\mathbf{x}}, \quad \text{where, } \boldsymbol{\varphi} = \boldsymbol{\theta}\mathbf{D} \tag{2}$$

where $\boldsymbol{\theta} \in \mathbb{R}^{p \times m}$ is the measurement matrix which is the binary sensor location matrix. That is, only one element of each row of the $\theta$ matrix contains the value 1 depending on the location of sensor and other values will be 0. As $p << m$ in $\theta$, hence recovering original response $\mathbf{y}$ of length $m$ from $p$ measurement in $\mathbf{z}$ is an under-determined problem. $\hat{\mathbf{x}}$ is the sparse representation of $\mathbf{z}$ in the sub-dictionary of $\mathbf{D}$ basis, i.e., $\boldsymbol{\varphi}$ .$\hat{\mathbf{x}}$ can be obtained exactly by solving an optimization problem as follows,

$$\min_{\hat{\mathbf{x}}} \| \mathbf{z} - \boldsymbol{\varphi}\hat{\mathbf{x}} \|_F^2 \quad \text{s.t. } \| x_j \|_0 < T \ \forall j \tag{3}$$

where $\| \cdot \|_0$ is the $L_0$ norm and $T$ is the sparsity level. $F$ denotes the Frobenius norm. As with dictionary learning, we use the Orthogonal Matching Pursuit (OMP) algorithm (Tropp and Gilber,

2007) to solve this optimization. Once $\hat{\mathbf{x}}$ is obtained, we can reconstruct the full-filed data by solving the forward problem,

$$\hat{\mathbf{y}} = \mathbf{D}\hat{\mathbf{x}} \tag{4}$$

The determination of sensor location presents a challenge because selecting a limited number of sensor nodes from the full set of available sensors is a combinatorial problem. Additionally, possible sensor location is inherently sparse. These motivates us to reformulate the dictionary learning into a sparse binary multi-objective optimization problem as follows:

$$\min \|\boldsymbol{\Theta}\|_0 \text{ and } \max\ r(\mathbf{y},\tilde{\mathbf{y}}) \tag{5}$$

where $r$ refers to the Pearson's correlation between the reconstructed and original training/testing measurements. A larger value of $r$ leads to more accurate reconstruction. Since the optimization algorithm operates on a one-dimensional vector but the reconstruction process requires a sparse matrix, a vectorization-reshaping mechanism is introduced. In this process, $\boldsymbol{\Theta}$ is a sparse selection matrix, which is vectorized into a binary vector $\boldsymbol{\theta}$ for optimization. The vector $\boldsymbol{\theta}$ is then reshaped back into the matrix form $\boldsymbol{\Theta}$ for use in the reconstruction process. For example, suppose $\boldsymbol{\theta}$ is a binary vector of size 12, where only the 3rd, 4th, and 7th entries are 1 (means that the limited measurements are obtained from sensors located at these 3 locations), while all other entries remain 0. The corresponding measurement matrix $\boldsymbol{\Theta}$ is constructed by reshaping this vector into a sparse matrix, where each row corresponds to a selected sensor. The vectorization-reshaping process can be illustrated as follows:

$$\boldsymbol{\Theta}:\begin{bmatrix} 0 & 0 & 1 & 0 & 0 & 0 & 0 & 0 & 0 & 0 & 0 & 0 \\ 0 & 0 & 0 & 1 & 0 & 0 & 0 & 0 & 0 & 0 & 0 & 0 \\ 0 & 0 & 0 & 0 & 0 & 0 & 1 & 0 & 0 & 0 & 0 & 0 \end{bmatrix} \underset{\text{reshaping}}{\overset{\text{vectorization}}{\rightleftharpoons}}$$

$$\boldsymbol{\theta}:\begin{bmatrix} 0 & 0 & 1 & 1 & 0 & 0 & 1 & 0 & 0 & 0 & 0 & 0 \end{bmatrix} \tag{6}$$

It is worth mentioning that selecting a few measurement points from dense measurement points for full-field data reconstruction is an underdetermined problem. Therefore, many solutions may exist. Fortunately, multi-objective optimization can also provide multiple solutions, which is precisely what we desire. From an engineering practical perspective, due to certain constraints, it may not be convenient to install sensors at certain locations. Hence, having multiple solutions offers more references for sensor placement. To solve the problem in Equation (5), the optimizer developed in our previous work will be adapted for current problem setting, as presented in the subsequent subsections. As shown in Figure 3, the flowchart summarizes the whole process of using limited measurements to reconstruct the full-filed structural responses based on dictionary learning. First, we obtain a dense measurement under controlled conditions. Subsequently, we train a dictionary using dictionary learning, which will be explained in the next sub-section. We then reframe the reconstruction process into a sparse binary multi-objective optimization, as shown in Equation (5), in which, a sparse coding is integrated, as shown in the bottom branch in Figure 3. After convergence or the iteration criteria are met, multiple solutions will be obtained.

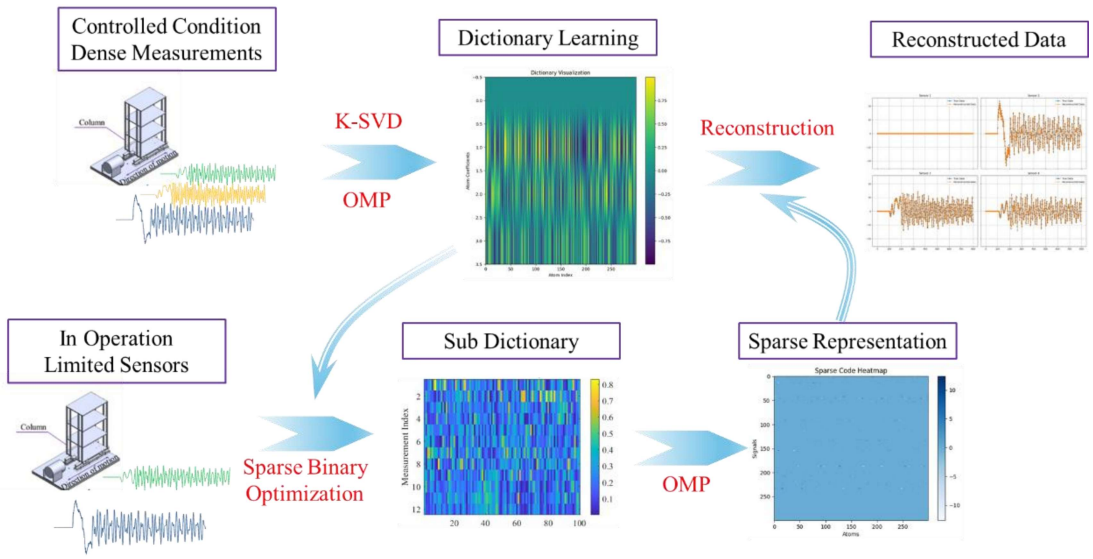


Figure 3.Flowchart of full-filed structural response reconstruction using limited data.

### 3.1.2 Binary particle swarm optimizer

This section describes the optimizer used to solve the reconstruction model formulated in the previous section. The model typically exhibits multimodality, meaning it contains multiple local extrema. Additionally, the presence of the L0 norm further increases its complexity. As a result, conventional gradient-based algorithms are not suitable for this problem. To address these challenges, we employ the Particle Swarm Optimization (PSO) technique (Kennedy and Eberhart, 1995), a type of population-based optimizer known for its simplicity, ease of implementation, and strong performance in multimodal problems. Given that our problem involves binary optimization, we adapt our previously developed Q-learning-enhanced PSO framework (Zhang et al, 2024). This framework was originally applied to structural damage identification with sparse, multimodal, and combinatorial characteristics, which share similarities with the current reconstruction setup. While the original framework was designed for continuous variable optimization, the binary nature of our reconstruction model necessitates specific modifications to the algorithm.

PSO was originally developed for continuous nonlinear optimization. The population of PSO is called a swarm, and each individual in the population of PSO is called a particle. A swarm consists of $N_p$ particles moving around a D-dimensional search space, each representing a potential solution. The *i*-th particle is characterized by its position vector $\mathbf{x}_i$ and velocity vector $\mathbf{v}_i$. Each particle flies through the solution space searching for the global optimal solution. In the process of flying, the current position and velocity of the *i*-th particle are updated according to the following equations, respectively:

$$\mathbf{v}_i^{k+1} = w \cdot \mathbf{v}_i^k + c_1 \cdot r_1 \cdot (\mathbf{p}_{\text{best},i}^k - \mathbf{x}_i^k) + c_2 \cdot r_2 \cdot (\mathbf{g}_{\text{best}}^k - \mathbf{x}_i^k) \tag{7}$$

$$\mathbf{x}_i^{k+1} = \mathbf{x}_i^k + \mathbf{v}_i^{k+1} \tag{8}$$

where $c_1$ and $c_2$ are the acceleration constants multiplied respectively by two random numbers, $r_1$ and $r_2$, uniformly distributed in [0.0, 1.0] and used to weight the velocity toward the best previous position of the *i*-th particle, $\mathbf{p}_{\text{best},i}^k$, and toward the best global position attained by all swarm members, $\mathbf{g}_{\text{best},i}^k$, found at iteration *k*. Parameter *w* is an inertia weight in interval [0.0, 1.0] to control

the influence of the previous velocity. A large inertia weight facilitates global exploration, which is particularly useful in the initial stages of an optimization. On the contrary, a small value allows for more localized searching, which is useful as the swarm moves toward the neighborhood of the optimum. A suitable value for the inertia weight usually provides a balance between exploration and exploitation and consequently results in a better optimum solution. A limit, $[\mathbf{v}_{\min}, \mathbf{v}_{\max}]$, may be placed on $\mathbf{v}_i$ to ensure that the velocities are acceptable. Velocities that are not within the range are clamped. In addition, the decision variable is bounded, $\mathbf{x}_i \in [\mathbf{x}_{\min}, \mathbf{x}_{\max}]$. If the updating equation causes the position to violate this interval, the infeasibility is removed by setting it to $\mathbf{x}_{\min}$ if $\mathbf{x}_i < \mathbf{x}_{\min}$ or equating it to $\mathbf{x}_{\max}$ if $\mathbf{x}_i > \mathbf{x}_{\max}$. However, it is known that the original PSO has difficulties in controlling the balance between exploration and exploitation and, therefore, has the disadvantage of premature convergence. Thus, we develop several local search heuristics to tackle the balance exploration and exploitation. To make the presentation clear, we revisit the five local search strategies and summarize them in Table 1.

Table 1.Local search heuristics.

| Strategy Name | Particle dynamics | Coefficients |
|---|---|---|
| Exploration | $v_i(t+1) = \omega v_i(t) + c_1 r_1 (p_{\text{best}i}(t) - x_i(t)) + c_2 r_2 (g(t) - x_i(t))$<br>$x_i(t+1) = x_i(t) + v_i(t+1)$ | $\omega = \omega_{\max} - \frac{(\omega_{\max} - \omega_{\min})it}{\text{maxIter}}$ $c_1 = 2.5$<br>$c_2 = 0.5$ |
| Convergence | $v_i(t+1) = \omega v_i(t) + c_1 r_1 (p_{\text{best}i}(t) - x_i(t)) + c_2 r_2 (g(t) - x_i(t))$<br>$x_i(t+1) = x_i(t) + v_i(t+1)$ | $\omega = \omega_{\max} - \frac{(\omega_{\max} - \omega_{\min})it}{\text{maxIter}}$ $c_1 = 0.5$<br>$c_2 = 2.5$ |
| Elitist-based perturbation | $tempP_{\text{best}i,d} = \begin{cases} P_{\text{best}i,d} + r_d \cdot (l_{\text{upper},d} - l_{\text{lower},d}) \\ if \ \text{rand} > 0.5 \\ P_{\text{best}i,d} - r_d \cdot (l_{\text{upper},d} - l_{\text{lower},d}) \\ if \ \text{rand} \le 0.5 \end{cases}$<br>repeated for defined times | $N \sim (\mu, R^2)$<br>$R = R_{\max} - \frac{(R_{\max} - R_{\min}) \cdot it}{\text{maxIter}}$ |
| Mutation | $tempL_{\text{best},d} = L_{\text{best},d} + normrnd(\mu, R^2)$<br>repeated for defined times | $N \sim (\mu, R^2)$<br>$R = R_{\max} - \frac{(R_{\max} - R_{\min}) \cdot it}{\text{maxIter}}$ |
| Fine Tuning | $tempP_{\text{best}i,d} = P_{\text{best}i,d} + V_{i,d}$<br>repeated for all dimensions | ——— |

Based on PSO, a binary version (BPSO) is proposed by Kennedy and Eberhart (1997) to accommodate discrete binary variables and allow it to operate in a binary problem space. A particle moves in a search space restricted to 0 or 1 on each dimension. In BPSO, updating a particle represents changes of a bit which should be in either state 1 or 0, and the velocity represents the probability of the bit taking the value 1 or 0. A sigmoid function is used to transform all real-

valued velocities to the range [0.0, 1.0]. In BPSO, the updating velocity equation remains unchanged while the position updating rule is replaced by the following equation:

$$\mathbf{x}_i^{k+1} = \begin{cases} 0 & \text{if rand}() \geq S(\mathbf{v}_i^{k+1}) \\ 1 & \text{if rand}() < S(\mathbf{v}_i^{k+1}) \end{cases} \tag{9}$$

where $S(\cdot)$ is a sigmoid function to transform the particle's velocity to the probability as follows:

$$S(\mathbf{v}_i^{k+1}) = \frac{1}{1+e^{-\mathbf{v}_i^{k+1}}} \tag{10}$$

and rand() is a random number uniformly distributed in [0.0, 1.0].

Leveraging the concept of BPSO, we can modify the local heuristics in Table 1 to address binary models formulated in Section 3.1. The particle velocity update equation remains the same, so only the position update equation needs adjustment. During iterations, *Exploration* and *Convergence* involve only changes in coefficients, the basic updating equations are the same as conventional PSO. The binary cases for *Exploration* and *Convergence* adopt Equations (15) and (16). While in the *EBP*, we directly alter the personal best position. It is worth noting that the best personal position in optimization is a binary vector as mentioned in Equation (12), therefore, the objective of *EBP* (Elitist-based perturbation) is to mutate the personal best by selecting one dimension and flipping a bit in its binary position, turning a 0 to 1 or 1 to 0. This process can be achieved and expressed as $\mathbf{p}_{\text{best},i,d}^{\text{temp}} = 1 - \mathbf{p}_{\text{best}i,d}^{k}$ directly. *Mutation* is similar to *EBP*, the bit-flipping expression is $\mathbf{g}_{\text{best},d}^{\text{temp}} = 1 - \mathbf{g}_{\text{best},d}$. For *Fine Tuning*, each dimension is flipped using a probabilistic strategy as shown in Equations (17) and (18). The flipping probability determines the likelihood of changing a bit in the binary position vector, adding variability and enabling exploration of new solutions.

$$\mathbf{x}_i^{k+1} = \begin{cases} 1\text{-}\mathbf{x}_i^k & \text{if rand}() < P_{\text{flip}} \\ \mathbf{x}_i^k & \text{otherwise} \end{cases} \tag{11}$$

The probability of flipping a bit, denoted as $P_{\text{flip}} = b/t^r$, is calculated with $b$ as the base probability. If the updated solution shows improvement, the probability is reset to $b$. Otherwise, it is reduced using a reduction factor $s$:

$$prob = \begin{cases} b & \text{if } \mathbf{x}_i^{k+1} \prec \mathbf{x}_i^k \\ prob / s & \text{otherwise} \end{cases} \tag{12}$$

where, $b$ is set to 0.5, $s$ is 4, $r$ is 5, and $t$ is 2 tuned with good performance on the reconstruction. By decaying the probability over time, we can reduce the chance of flipping. This can help maintain the structure of the optimal solution currently found while still allowing for some level of exploration.

## 3.2 Full-field reconstruction case demonstration

This section demonstrates the proposed reconstruction framework through two case studies. Case I examines reconstruction under the same loading condition, where both dictionary training and reconstruction use burst chirp excitation data. Case II explores cross-loading reconstruction scenarios, where the dictionary is trained under one loading condition and applied to reconstruct responses under a different excitation. These cases validate the method's effectiveness and robustness for practical engineering applications.

### 3.2.1 Case I: Reconstruction under the Same Loading Condition

In Case I, a burst chirp signal covering 3-25 Hz is used to excite the structure over 2 seconds. The sampling frequency is set to 400 Hz, yielding 800 data points per time series. The vibrometer outputs velocity responses directly, which are used for both training and reconstruction. Two independent datasets are collected: one for dictionary training and one for testing reconstruction accuracy. The dictionary is randomly initialized and trained using the first dataset. Figure 4 shows the initialized and learned dictionaries, where each heatmap represents a dictionary matrix (16 spatial locations × 100 atoms). These atoms serve as basis functions encoding spatial dependencies across measurement locations. The dictionary captures compressed spatial relationships rather than direct vibration patterns, enabling response reconstruction from limited measurements.

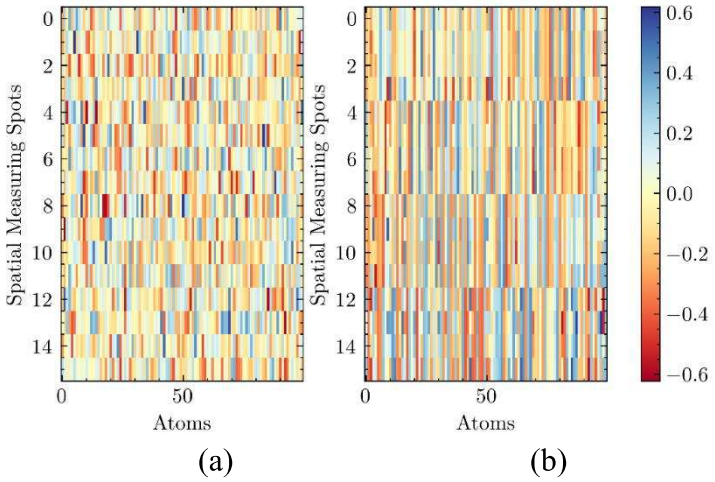


Figure 4.(a) Initialized dictionary and (b) learned dictionary for burst chirp excitation.

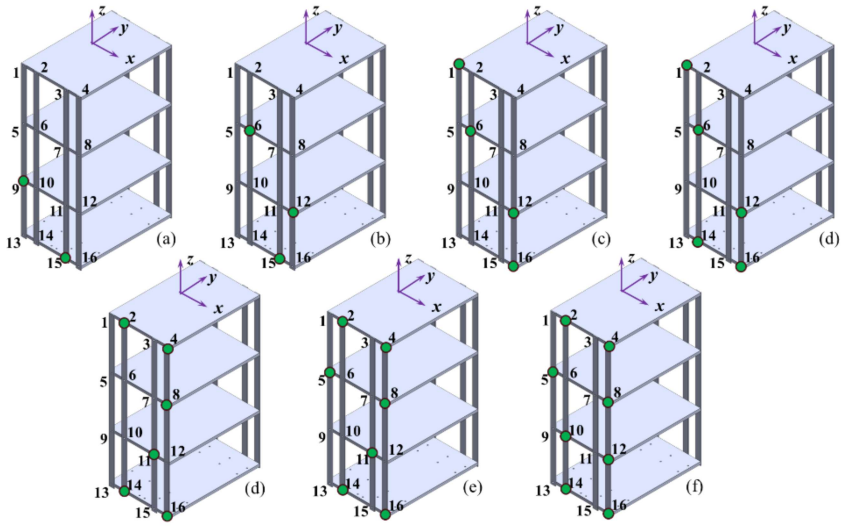


Figure 5. Multiple optimal solutions for limited sensor layout.

The reconstruction process is formulated as a multi-objective binary optimization problem, yielding multiple solutions with different sensor placement configurations and varying sensor

counts. To simulate resource-constrained scenarios, a maximum of eight sensors is imposed. Seven optimal solutions are obtained (Figure 5), with sensor counts ranging from 2 to 8. Each solution corresponds to specific sensor locations marked by green dots, where measurements enable full-field response reconstruction with varying accuracy levels. To verify solution optimality, perturbations are introduced to each optimal solution, generating alternative sensor placements with the same sensor count but different locations (Table 2). Reconstruction accuracy is quantified using average similarity across all 16 locations, defined as the mean Pearson correlation coefficient between reconstructed and ground truth responses.

Table 2. Sensor placement combinations from optimization and perturbations for Case I.

| Solutions | Optimization | Mutated 1 (Random 1) | Mutated 2 (Random 2) |
|---|---|---|---|
| Sol 1 | 9, 15 | 2, 7 | 8, 14 |
| Sol 2 | 6, 12, 15 | 7, 9, 14 | 2, 5, 11 |
| Sol 3 | 1, 6, 12, 16 | 4, 7, 13, 16 | 1, 9, 10, 13 |
| Sol 4 | 1, 6, 12, 14, 16 | 1, 7, 12, 14, 16 | 1, 7, 12, 13, 16 |
| Sol 5 | 2, 4, 8, 11, 14, 16 | 2, 4, 9, 11, 14, 16 | 2, 3, 9, 11, 14, 16 |
| Sol 6 | 2, 4, 5, 8, 11, 14, 16 | 2, 4, 6, 8, 11, 14, 16 | 2, 4, 6, 8, 11, 13, 16 |
| Sol 7 | 2, 4, 5, 8, 10, 12, 14, 16 | 2, 3, 5, 8, 10, 12, 14, 16 | 2, 4, 5, 8, 10, 12, 13, 16 |

Figure 6 presents the average similarity comparisons between the optimal solutions and their perturbations. The horizontal axis denotes the solution index, while the vertical axis indicates the average similarity across 16 locations, which serves as the accuracy metric in this study. The solutions differ in the number of sensors used, ranging from 2 to 8 (Sol1 to Sol7) out of the 16 locations, thereby reflecting different levels of sensor sparsity. Each optimal solution is accompanied by two perturbed variations, resulting in three bars per solution. Regardless of how the solutions are perturbed, their reconstruction accuracies never exceed those of the optimal solutions. This confirms that the solutions obtained through the optimization algorithm are indeed optimal. Additionally, we analyze the relationship between reconstruction accuracy and the number of sensors, as visualized by the curve in Figure 8. As expected, increasing the number of sensors improves accuracy. Intuitively, more sensors provide more information, leading to more precise reconstructions. However, our objective is to achieve high-accuracy reconstruction with a limited number of sensors, which is why we impose an upper limit of eight. Furthermore, we explore whether a smaller number of sensors can still meet the accuracy requirements. From the curve, we observe that a solution using only five sensors (Sol 4) achieves an average similarity of 0.9933. As the number of sensors increases to six and seven, the average similarity rises to 0.9985 and 0.9993, corresponding to marginal accuracy improvements of 0.5% and 0.6%, respectively. This suggests that the similarity metric has nearly converged. Notably, the average similarity itself reaches a high level, approaching 1.

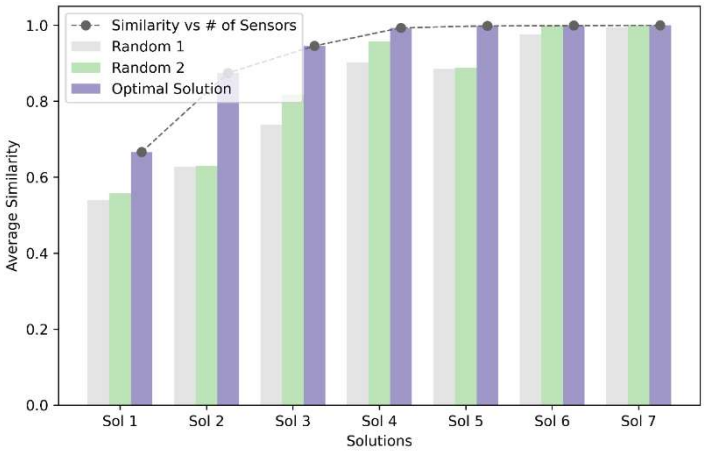


Figure 6. Average similarity comparison between different solutions

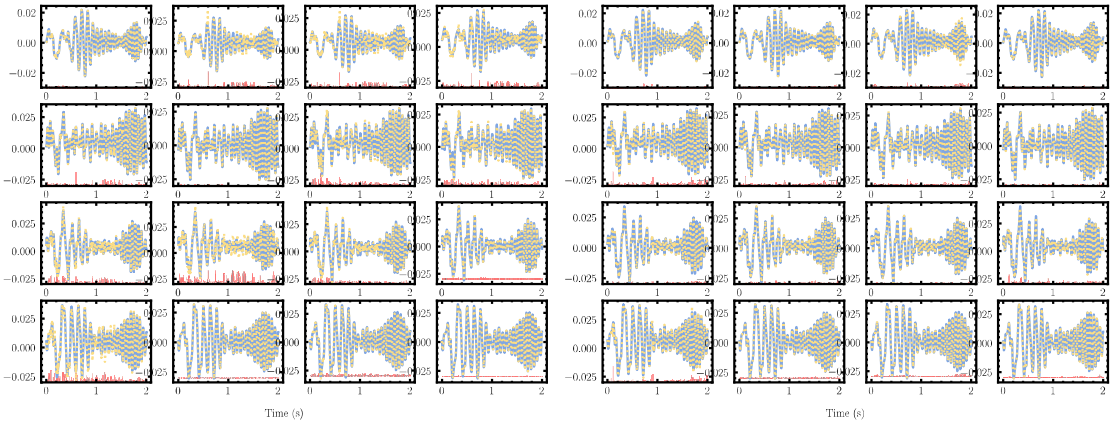


(a) Sol 4 with 5 sensors. (b) Sol 5 with 6 sensors.

Figure 7. Vibration comparison with ground truth. Blue solid line is ground truth, and orange dash line is reconstruction. The subplots, arranged from the upper left to the bottom right, correspond to measurement locations 1 through 16.

To comprehensively evaluate reconstruction quality, time-series comparisons and error distributions are examined. Figure 7 compares Solutions 4 (5 sensors) and 5 (6 sensors). In Solution 4, reconstructions generally capture structural vibrations accurately, but miss some peaks at locations 2-4, 9-11, and 13, particularly during initial excitation. This discrepancy is attributed to complex frequency variations and transient dynamics at excitation onset. In contrast, Solution 6 with 6 sensors shows near-perfect agreement, fully recovering the missing details. The error bars across all time points exhibit notably smaller fluctuations for Solution 5, demonstrating superior reconstruction performance.

Three representative data-driven algorithms are selected for comparison: autoencoder, transformer (two deep learning approaches), and Karhunen-Loève transformation (KL/POD, a decomposition-based method). Using the 6-sensor configuration (Solution 5) on Case I dataset, the autoencoder, our approach, transformer, and KL/POD achieve average similarities of 0.9989, 0.9985, 0.999, and 0.9993, respectively (Table 3). While achieving comparable accuracy, our

approach offers significant practical advantages: (1) no retraining required when sensor configurations change, unlike deep learning models that must be retrained for different input dimensions; (2) operational flexibility maintaining performance regardless of input dimensions; (3) architectural simplicity requiring no design modifications for specific applications. Additionally, cross-domain evaluation reveals that KL/POD performs well within the same signal domain but cannot effectively reconstruct across different excitations (burst-to-sine or sine-to-burst), whereas our method maintains robust performance across varying loading conditions.

Table 3. Performance comparisons on Case I data.

| Approaches | Training time (on GPU) | Retraining | Input dimension dependance | Architecture design |
|---|---|---|---|---|
| Our approach | 17.38s(±1.15) | No | No | No |
| Autoencoder | 10.43s(±0.68) | Yes | Yes | Yes |
| Transformer | 47.71s (±0.65) | Yes | Yes | Yes |
| KL/POD | 1.36s (±0.11) | No | No | No |

### 3.2.2 Case II: Reconstruction under Different Loading Conditions

In practical applications, structures are monitored under varying loading conditions. Case II explores cross-loading reconstruction where dictionaries trained under one excitation are applied to reconstruct responses under different loading. Two scenarios are examined: burst-to-sine and sine-to-burst reconstruction. When the dictionary is trained using burst chirp data and applied to reconstruct sine excitation responses (near 5 Hz), the optimization yields 5 solutions (Figure 8). Solution 4 with 6 sensors achieves 0.9998 average similarity. Figure 9 shows that reconstructed curves match ground truth excellently across all 16 locations, with absolute relative errors nearly zero at all time points. This demonstrates that dictionaries capture structural spatial response patterns rather than specific load characteristics, enabling accurate cross-loading reconstruction.

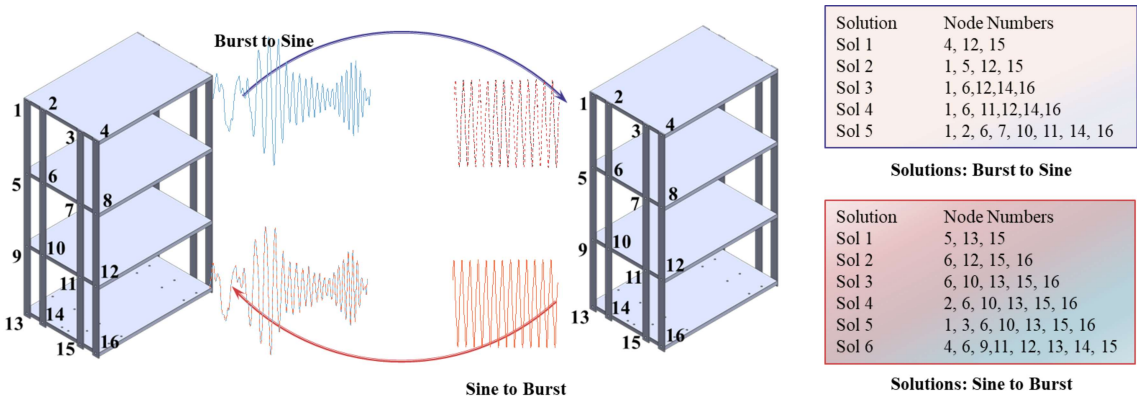


Figure 8. Schematic diagram for reconstructions under varying loadings.

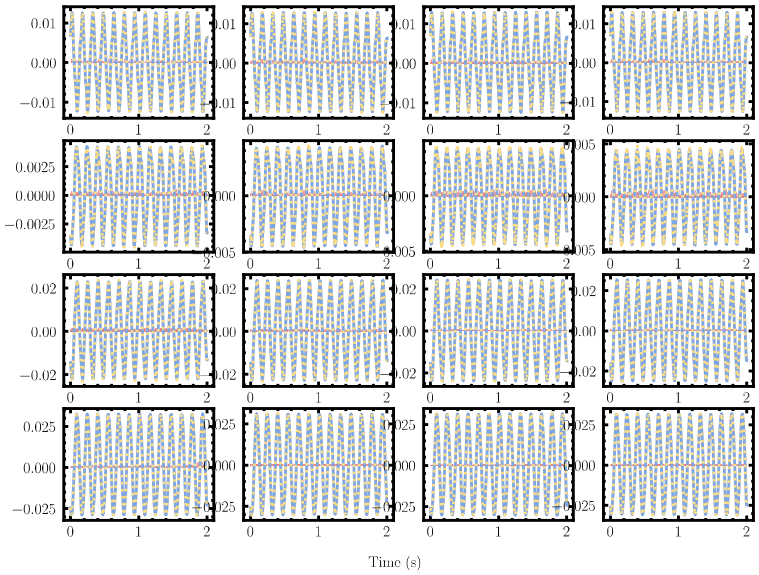


Figure 9. Response comparisons and error analysis for case of burst to sine. Reconstructed response comparisons using Solution 4 with 6 sensors.

When the dictionary is trained (Figure 10) using monotonic sine data and applied to reconstruct burst chirp responses, the optimization yields 6 solutions. Solutions 4, 5, and 6 using 6, 7, and 8 sensors achieve accuracies of 0.9527, 0.9687, and 0.985, respectively (deviations of 4.73%, 3.13%, and 1.5% from unity). Figure 11 shows that even with 8 sensors (Solution 6), reconstruction curves deviate from ground truth at locations 3, 4, 5, 9, 11, and 12, with high error fluctuations across time points. This limitation arises because dictionaries trained on monotonic signals cannot capture response patterns from broader frequency excitations. The finding emphasizes that rich, diverse training data covering various loading conditions is essential for achieving high-fidelity cross-loading reconstruction in real-world applications.

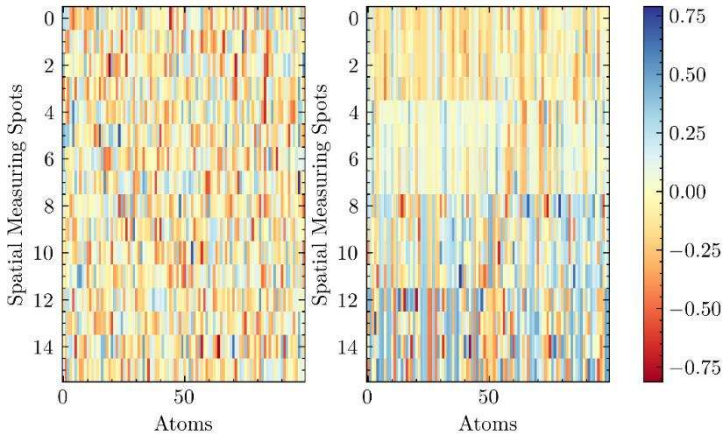


(a) (b)

Figure 10. (a) Initial dictionary and (b) learned dictionary for sine excitation.

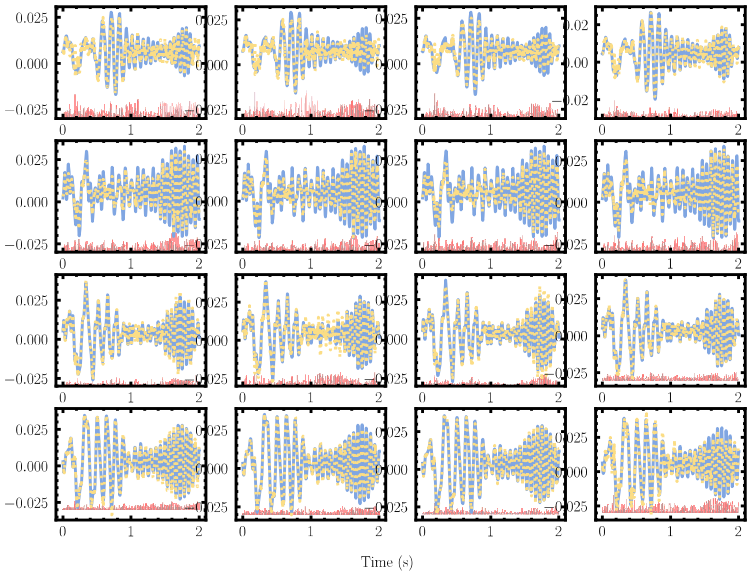


Figure 11. Response comparisons and error analysis for case of sine to burst. Reconstructed response comparisons using Solution 6 with 8 sensors.

### 3.3 Application to Structural Damage Detection

The application of full-field response reconstruction to damage identification is grounded in two fundamental principles. First, from the dictionary learning perspective, the trained dictionary captures structural spatial response patterns rather than load-specific vibration signatures. Consequently, the dictionary can reconstruct full-field responses under various loading conditions, as demonstrated by the burst-to-sine reconstruction in Section 3.2. Second, if the structure is time-invariant (i.e., in healthy condition), the reconstructed responses should yield consistent dynamic characteristics (natural frequencies, mode shapes, and damping ratios) regardless of excitation type. However, when structural damage occurs, these mechanical properties change due to local stiffness reduction, manifesting as shifts in natural frequencies and alterations in mode shapes. These changes enable damage localization through modal-based indicators. An important aspect is that reconstruction can be performed regardless of the structure's health state. The mathematical principle underlying reconstruction (Equation 1) states that any engineering signal can be represented as a linear combination of dominant basis functions. As long as the dictionary contains corresponding vibration modes, reconstruction remains feasible. Under damaged conditions, the primary difference compared to the healthy state is that the coefficients of the linear combination change, reflecting the altered structural response patterns.

A numerical simulation model is established based on the three-story laboratory structure. To introduce structural damage, the thickness of one support column between the 1st and 2nd floors (connecting points 6 and 10) is reduced from 3.175 mm to 2.675 mm, as shown in Figure 12. Due to structural symmetry, the corresponding column on the opposite side is also damaged. This damage scenario is widely adopted in structural health monitoring studies, effectively simulating practical conditions such as material degradation, corrosion, or fatigue-induced cross-sectional reduction. The structure is equipped with 16 sensors (4 per floor, numbered sequentially left to right). The shaker generates chirp waveform excitation with 5 mm displacement amplitude over approximately 4 seconds. Under both healthy and damaged conditions, displacement responses from all sensors are recorded. To simulate real-world measurement uncertainties, Gaussian white

noise with 15% magnitude relative to signal standard deviation is added to the damaged structural response data.

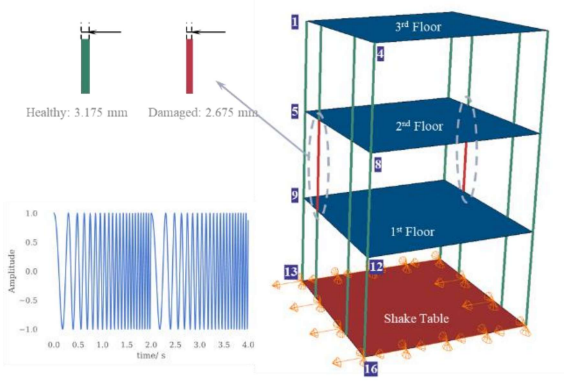


Figure 12. Schematic illustration of simulation modeling.

Dictionary learning and multi-objective optimization are employed for reconstruction and optimal sensor placement. The healthy dataset trains the dictionary, while the noisy damaged data undergoes reconstruction. One optimal solution places sensors at locations 3, 6, 8, 10, 14, and 16, achieving 0.999583 average similarity between reconstructed signals and ground truth across all 16 locations. Modal identification is performed on both partial measurements and fully reconstructed data. Under healthy conditions with full measurements, the identified natural frequencies are 5.1270 Hz and 14.4043 Hz. Under damaged conditions, these frequencies shift to 4.8828 Hz and 14.1602 Hz. For damage localization, two modal-based indicators are employed: Coordinate Modal Assurance Criterion (COMAC) and modal flexibility change. COMAC identifies which degrees of freedom (DOF) negatively contribute to modal correlation, where values near 1 indicate intact structure and values near 0 signify damage. Modal flexibility increases locally at damage locations due to stiffness reduction. A combined indicator (1 - COMAC) × flexibility change is computed, where measurement DOFs with maximum values correspond to damage locations.

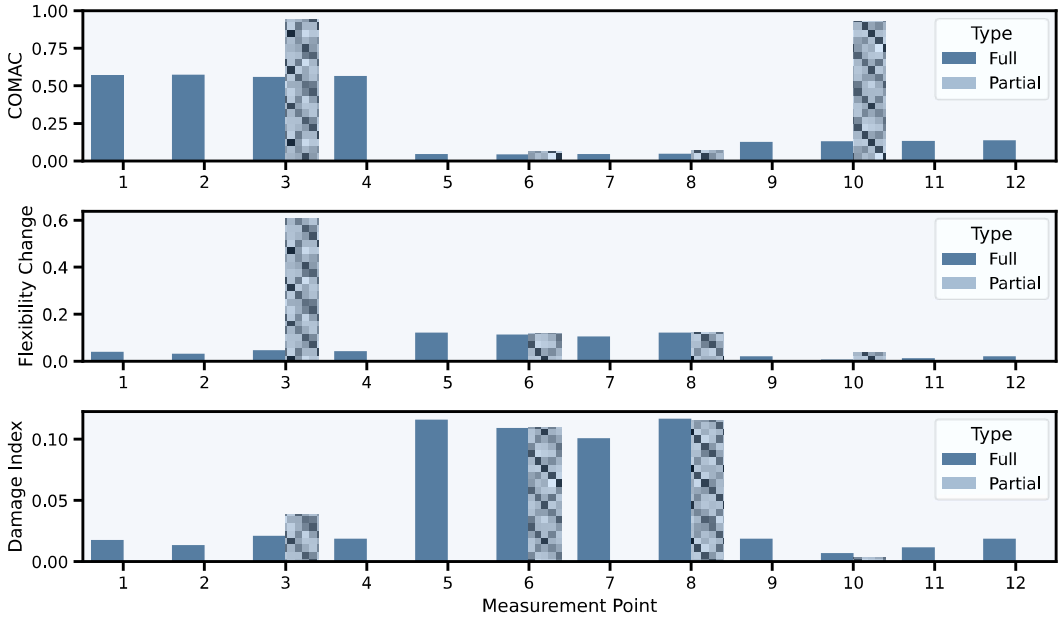


Figure 13. Damage localization indicators using partial and fully reconstructed responses.

Figure 13 presents damage localization indicators using fully reconstructed responses. Since DOFs 13-16 correspond to input nodes, they are excluded from calculations. The COMAC indicator shows that DOFs 5-8 exhibit the lowest values, suggesting damage in this region. The flexibility change indicator shows DOFs 5-8 with the highest values, followed by DOFs 9-12, strongly indicating second-floor damage. The comprehensive indicator product clearly identifies DOFs 5-8 as most affected, followed by DOFs 9-12. The ground truth confirms damage at the column connecting DOFs 6 and 10, validating the accuracy of full-field reconstruction-based damage localization. In contrast, damage detection using only partial measurements from sensors 3, 6, 8, 10, 14, and 16 yields incomplete results. Although partial data captures some damage information (significant anomaly at location 7, followed by location 11, suggesting second-floor damage), it fundamentally lacks a global structural perspective. Most indicator values are zero due to unmeasured locations. This limitation creates significant blind spots, potentially leading to incomplete damage assessment and misdiagnosis. The absence of data at critical locations prevents accurate identification of complete damage patterns and their spatial relationships.

The comparison demonstrates that full-field data reconstruction provides comprehensive and reliable structural health assessment by generating damage indices at all measurement points. This holistic approach enables engineers to visualize complete damage patterns, identify precise locations, and understand damage propagation throughout the structure. The ability to generate indices for unmeasured points through reconstruction significantly enhances practical applicability of structural health monitoring systems, particularly in complex structures where sensor placement is limited by physical or economic constraints. Therefore, full-field reconstruction represents a promising approach for practical engineering applications, balancing monitoring accuracy with implementation feasibility.

The case studies demonstrate that the proposed method yields multiple solutions providing valuable guidance on sensor placement and optimal sensor count. The availability of multiple solutions offers operational flexibility when certain sensors fail or specific locations are unsuitable for installation. The validation confirms that just 6 strategically placed sensors can achieve accurate full-field response reconstruction regardless of excitation type. The approach has been successfully validated using different response types (acceleration, displacement, velocity) and can be extended to other signatures such as strain or stress through appropriate dictionary training. With rich training data covering various conditions, accurate reconstruction of in-service structural responses is achievable. The downstream damage detection results emphasize that full-field reconstructions are essential for accurate damage localization in structural health monitoring applications.

# Chapter 4: Education Impact and Knowledge Dissemination

Throughout this project, three graduate students are involved at different stages of research. Yang Zhang set up the testbed and conducted data acquisition. Ting Wang looked into shaker excitation and contributed to sensor integration. Yang Zhang and Qianyu Zhou worked together on sensor network optimization and full-field re-construction algorithm based on machine learning. They collaborated on damage detection case demonstration. The work is heavily experimental. All these students gained significant amount of experiences on sensor tuning, information fusion, machine learning, and decision making for structural fault detection. The research components have been incorporated to their respective Ph.D. dissertations. Yang Zhang and Ting Wang received Ph.D. degrees during the duration of the project. Qianyu Zhou is progressing well in his Ph.D. study, and is expected to graduate in the fall of 2025.

The research findings have been integrated into several undergraduate- and graduate-level classes that the PI has instructed in project years, including ME3220 Mechanical Vibrations, ME 5420 Advanced Mechanical Vibrations, ME 5210 Intelligent Material Systems and Structures, and ME 5895 Structural Dynamics.

The research outcome has been presented systematically in TIDC annual review meetings and poster competitions. The key research findings are being summarized into archival publications.

# Chapter 5: Conclusions and Recommendations

The overarching goal of this research is to synthesize a new framework of infrastructure monitoring that can concurrently take in sensing signals from both traditional sensors and new sensing techniques, process the information through machine learning that integrate together deep learning and underlying physics, and produce highly accurate and robust full field measurement results to facilitate fault detection. This goal has been successfully achieved.

Our findings are the following:

- Different sensors possess different levels of sensitivity toward structural damage detection and identification. In general, sensors and sensing devices with high-frequency interrogation capability possess higher detection sensitivity. At the same time, higher detection sensitivity may lead to higher likelihood of false alarms. As such, mitigating strategy will be beneficial.
- Data-driven techniques built upon machine learning can offer significant detection robustness in general, as they can bypass the challenges in variations and uncertainties with respect to the underlying baseline numerical model that are inherent in measurements.
- Full-field measurements provide critical insights into structural behavior, enabling comprehensive analysis of deformation, vibration, and stress distributions etc. However, the reality is that sparse sensor measurements are typically the case in practical applications. Therefore, reconstructing full-field measurement based on a small number of point sensors becomes necessary.
- The proposed approach that integrates dictionary learning into a sparse binary multi-objective optimization framework to reconstruct full-field structural responses is extremely promising. A case study on a three-story laboratory testbed structure demonstrated the effectiveness its effectiveness. The results reveal that (1) the framework successfully identifies multiple sensor combinations, each yielding accurate reconstructions of the full-field response; and (2) the reconstructed data align closely with the true measurements, validating the feasibility and accuracy of the framework.
- The reconstructed full-field measurement can lead to successful structural fault detection.

The research outcomes lay down a foundation for engineering implementation for infrastructure monitoring. In order to fully unleash the potential of the new technology, we envision the following further advancements:

- The scope of work can be extended to larger and more complex structures,
- We can leverage physical modeling or simulation-generated data as training inputs to enhance generalizability. The method's inherent flexibility allows for adaptation to different response types (acceleration, displacement, strain) and structural configurations through appropriate dictionary training.
- The reconstructed full field measurement can potentially lead to damage localization and even severity assessment.

## References

Ao, C., Qiao, B., Liu, M., Zhu, W., Zhu, Y., Wang, Y. and Chen, X., 2023. Non-contact full-field dynamic strain reconstruction of rotating blades under multi-mode vibration. Mechanical Systems and Signal Processing, 186, p.109840.

Jana, D. and Nagarajaiah, S., 2023. Data-driven full-field vibration response estimation from limited measurements in real-time using dictionary learning and compressive sensing. Engineering Structures, 275, p.115280.

Kennedy, J. and Eberhart, R., 1995, November. Particle swarm optimization. In Proceedings of ICNN'95-International Conference on Neural Networks (Vol. 4, pp.1942-1948). IEEE.

Kennedy, J. and Eberhart, R.C., 1997, October. A discrete binary version of the particle swarm algorithm. In 1997 IEEE International Conference on Systems, Man, and Cybernetics. Computational Cybernetics and Simulation (Vol. 5, pp.4104-4108). IEEE.

Mousavi, Z., Varahram, S., Ettefagh, M.M. and Sadeghi, M.H., 2023. Dictionary learning-based damage detection under varying environmental conditions using only vibration responses of numerical model and real intact state: Verification on an experimental offshore jacket model. Mechanical Systems and Signal Processing, 182, p.109567.

Rubinstein, R., Zibulevsky, M. and Elad, M., 2008. Efficient implementation of the K-SVD algorithm using batch orthogonal matching pursuit (No. CS Technion report CS-2008-08). Computer Science Department, Technion.

Tropp, J.A. and Gilbert, A.C., 2007. Signal recovery from random measurements via orthogonal matching pursuit. IEEE Transactions on Information Theory, 53(12), pp.4655-4666.

Wei, D., Chen, Y., Li, H. and Zhang, X., 2023. Real-time reconstruction method of full-field dynamic response of rotating bladed disks. Mechanical Systems and Signal Processing, 188, p.109953.

Yuan, J., Szydlowski, M. and Wang, X., 2024. An optimal sparse sensing approach for scanning point selection and response reconstruction in full-field structural vibration testing. Mechanical Systems and Signal Processing, 212, p.111298.

Zhang, Y., Zhou, K. and Tang, J., 2024. Piezoelectric impedance-based high-accuracy damage identification using sparsity conscious multi-objective optimization inverse analysis. Mechanical Systems and Signal Processing, 209, p.111093.


Transportation Infrastructure Durability Center
AT THE UNIVERSITY OF MAINE

35 Flagstaff Road
Orono, Maine 04469
tidc@maine.edu
207.581.4376

**www.tidc-utc.org**